processes

MDPI

Article

Synthesis and Characterization of Chitosan-Silver Particles: Exploratory Evaluation of Their Antibacterial Activity Against *Bacillus halotolerans* MCC1 from the Sea of Cortes

Valeria Adilene Acosta-Misquez [1], Jesús Álvarez-Sánchez [1,*], Germán Eduardo Dévora-Isiordia [1], Yedidia Villegas-Peralta [1,*], Reyna Guadalupe Sánchez-Duarte [1], Beatriz Guadalupe González-González [2], Sergio Perez-Sicairos [3] and Lorenzo A. Picos-Corrales [4]

[1] Departamento de Ciencias del Agua y Medio Ambiente, Instituto Tecnológico de Sonora, 5 de febrero 818 Sur, Ciudad Obregón 85000, Mexico; valeria.misquez@gmail.com (V.A.A.-M.); german.devora@itson.edu.mx (G.E.D.-I.); reyna.sanchez@itson.edu.mx (R.G.S.-D.)
[2] Departamento de Biotecnología y Ciencias Alimentarias, Instituto Tecnológico de Sonora, 5 de febrero 818 Sur, Ciudad Obregón 85000, Mexico; beatriz.gonzalez@itson.edu.mx
[3] Centro de Graduados, Instituto Tecnológico de Tijuana, Blvd. Alberto Limon Padilla y Av. ITR de Tijuana, s/n Mesa de Otay, Tijuana 22500, Mexico; sergio.perez@tectijuana.edu.mx
[4] Facultad de Ingeniería Culiacán, Universidad Autónoma de Sinaloa, Ciudad Universitaria, Av. Josefa Ortiz de Dominguez S/N, Culiacan 80013, Mexico; lorenzo.picos.c@uas.edu.mx
* Correspondence: jesus.alvarez@itson.edu.mx (J.Á.-S.); yedidia.villegas@itson.edu.mx (Y.V.-P.); Tel.: +52-644-4100-900 (ext. 1689) (J.Á.-S.)

Abstract

Currently, advances in technology and research make it possible to valorize shrimp waste to synthesize advanced materials. In addition, this valorization helps reduce the environmental impact caused by improper handling. Therefore, this research addresses the synthesis and characterization of chitosan-silver particles (C-Ag Ps), a promising approach to develop materials with antibacterial potential by combining the properties of chitosan and silver using the ionic gelation technique. The C-Ag Ps were characterized using dynamic light scattering (DLS), scanning electron microscopy (SEM), Fourier-transform infrared spectroscopy (FTIR), X-ray diffraction (XRD), thermogravimetric analysis (TGA), and atomic force microscopy (AFM). Antibacterial tests were conducted with C-Ag Ps concentrations of 0.05, 0.10, and 0.15 mg mL^{-1} at 30 °C against *Bacillus halotolerans* MCC1. The DLS results indicated that the C-Ag Ps had a particle diameter of 168.8 nm while SEM showed an average size of 116.92 nm; XRD analysis revealed that the peaks at 27.94°, 32.25°, 46.37°, 55°, 57°, and 67° indicate that the Q-Ag particles contain AgCl. TGA analysis showed that the C-Ag Ps exhibited an inorganic residue of 52.66% at 600 °C. Furthermore, an increase in antibacterial activity was observed as the concentration of C-Ag Ps increased.

Keywords: biofouling; chitosan-silver; ionic gelation; particles; DLS; SEM

Check for updates

Academic Editor: Paolo Trucillo

Received: 7 October 2026
Revised: 6 November 2026
Accepted: 14 November 2026
Published: 18 November 2026

Copyright: © 2026 by the authors. Licensee MDPI, Basel, Switzerland. This article is an open access article distributed under the terms and conditions of the Creative Commons Attribution (CC BY) license.

1. Introduction

Hybrid particles have experienced an unprecedented boom due to the properties derived from their components [1,2]. Numerous studies have focused on optimizing particle properties using preparation methods that promote various inter- and intramolecular interactions. In this regard, biopolymers have emerged as a highly attractive option for producing hybrid particles because of their biodegradability and biocompatibility. This group includes natural and synthetic derivatives of proteins, polypeptides, and polysaccharides, with chitosan playing a prominent role in recent years [3,4]. Hybrid particles

have attracted the research community because of their wide range of potential applications in medicine, nanotechnology, biochemistry, and environmental sciences [5–9]. Because they are very small, they have a larger surface area per unit mass; that is, the number of atoms on the surface increases exponentially as their size decreases [10]. In addition, particle size depends on the synthesis technique used to produce them. Various physical, chemical, and biological methods can synthesize them, including ionic gelation, which relies on electrostatic interactions between a positively charged polymer (e.g., chitosan, C) and a multivalent cross-linking agent with an opposite charge (e.g., tripolyphosphate, TPP). In this method, ionic gelation forms noncovalent and coordinated bonds, resulting in small particles [11]. This technique allows size control through ionic interactions between chitosan and cross-linking agents. As is well known, numerous classifications exist based on composition, shape, and size. In particular, chitosan-silver particles (C-Ag Ps) fall under the category of hybrid particles [12,13], alongside other types of particles, including metallic particles, metal-oxide-derived particles, and carbon-based particles [14,15]. As key advantages, the ionic gelation method is a low-cost and scalable process and does not generate hazardous waste—which is beneficial for the environment, especially considering that the raw material used is derived from a waste product such as shrimp shells [16–18]; the C-Ag Ps can show antibacterial and antifungal properties, which can be attributed to several factors, such as their high surface-to-volume ratio, which enhances interaction with microorganisms, damages their membranes, and affects their DNA, ultimately leading to their death [19–21]. Therefore, ionic gelation has emerged as a promising strategy for preparing C-Ag Ps with enhanced physical, chemical, and biological properties, including their recognized antibacterial activity [22,23]. These particles have been extensively studied as bactericidal and fungicidal agents, especially in biotechnological applications and in processes where exponential microbial growth can lead to the formation of a biofouling layer or biofouling phenomenon [24,25]. In 2022, Torres-Valenzuela et al., modified reverse osmosis membranes with Ag nanoparticles (Ag NPs) using concentrations of 5, 10, and 15 mg in 100 mL, respectively. This successfully inhibited the growth of the bacterium *Bacillus halotolerans* MCC1 (Sea of Cortes COLMENA 1). The resulting nanoparticles significantly reduced the biofilm layer, total cell count, and total organic carbon on the surfaces of the modified membranes (72, 48, and 45%, respectively) [25]. In a study by Ali et al., [26], chitosan nanoparticles (C-NPs) with an average diameter of 115.5 ± 0.6 nm were obtained using the ionic gelation technique, where C-Ag NPs had a particle size of 165.8 ± 1.5 nm, as measured by DLS at pH 6.0. Meanwhile, Villegas-Peralta et al., discovered in 2020 [27] that particle size varies with chitosan molecular weight, so they used -low, medium-, and high-molecular-weight chitosan to synthesize the particles, and DLS provided the particle sizes yielding 420.0 ± 0.07, 550.5 ± 17.89, and 600.3 ± 55.58 nm, respectively. Lower chitosan molecular weight resulted in smaller chitosan particles. Additionally, particle diameter variation decreased as chitosan molecular weight decreased. The nanoparticles exhibited antibacterial activity against *Bacillus halotolerans* MCC1; nanoparticles made from high-molecular-weight chitosan (CSNP2) showed the best performance.

Based on the current literature, further exploration of the described systems is required. Therefore, this study aimed to synthesize chitosan-silver particles using the ionic gelation method and to conduct preliminary exploratory assays to evaluate their antibacterial activity against *Bacillus halotolerans* MCC1 isolated from the Sea of Cortes. To prepare the C-Ag Ps, we used the ionic gelation method with sodium tripolyphosphate (TPP) as the cross-linking agent, along with an aqueous silver nitrate solution and a laboratory-prepared chitosan solution. The resulting C-Ag Ps were comprehensively characterized using dynamic light scattering (DLS), SEM (scanning electron microscopy), AFM (atomic force microscopy), FTIR (infrared spectroscopy), X-ray diffraction (XRD), and thermogravimetric analysis

(TGA). Inhibition tests against the bacterium *Bacillus halotolerans* MCC1 were conducted in Petri dishes containing saline agar and C-Ag Ps at different concentrations of 0.05, 0.10, and 0.15 mg mL^{-1} at 30 °C.

2. Materials and Methods

2.1. Reagents

The substances used for particle synthesis included laboratory-synthesized chitosan (degree of deacetylation of 82.97%, high molecular weight of 501.59 kDa), silver nitrate ($AgNO_3$ > 99.9%) and sodium tripolyphosphate (TPP, >86%) purchased from Fermont (Monterrey, Nuevo León, Mexico). Nutrient agar was obtained from DIBICO (Cuautitlán Izcalli, State of Mexico, Mexico).

2.2. Synthesis of C-Ag Ps

The synthesis of C-Ag Ps began with dissolving chitosan (0.25 g) in an acidic medium (1% *v*/*v* acetic acid (AA)). After dissolving the chitosan in 150 mL of AA (0.167% *m*/*v*), the solution was filtered through a fine-mesh strainer. Next, 50 mL of TPP (0.116% *w*/*v*) was added, followed by 10 mL of 0.002 M silver nitrate (0.0344 g to a final volume of 100 mL distilled water). Both solutions were added at a flow rate of 10 mL min^{-1}, dripping from a height of 2 cm above the chitosan solution. The initial ratio used was Q-TPP 1:0.23 and Q-$AgNO_3$ 1:0.01376.

After the solutions had dripped in, the prepared solution was maintained at 1200 rpm for 30 min on a magnetic stirrer (VWR Model 200, San Francisco, CA, USA). Next, we decanted the solution into Falcon tubes and centrifuged it in an OHAUS Model FC 5706 (Parsippany, NJ, USA) at 5000 rpm for 40 min (equivalent to 3075× *g*). After obtaining the first precipitate, we washed it twice with distilled water and centrifuged it again for 20 min at the same rpm each time (Figure 1).

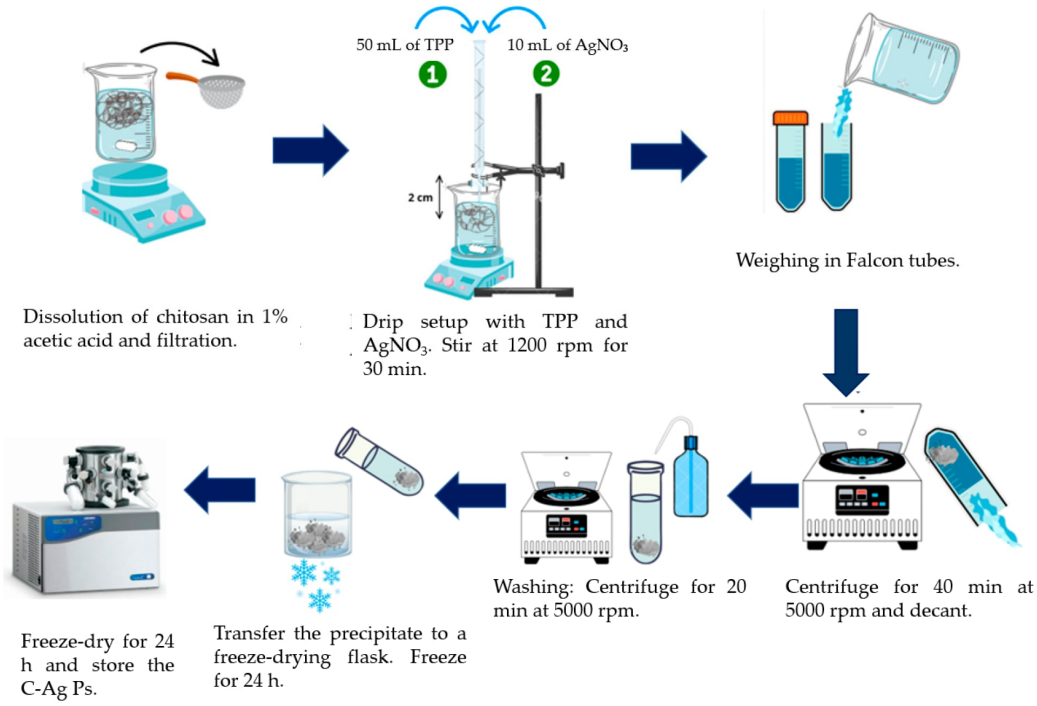


Figure 1. Synthesis of chitosan-silver particles (C-Ag Ps) by ionic gelation.

2.3. Characterization by DLS

To determine particle size, a dynamic light scattering (DLS) instrument (Anton Paar, model Litesizer DLS 500, Graz, Styria, Austria) was used, and the data were analyzed using Kalliope software (version 3.2.5, 2023). A solution was prepared as follows: 1 mg of C-Ag Ps was weighed and dispersed in a 1% v/v aqueous acetic acid solution. 3 mL of the prepared solution was drawn up using a Pasteur pipette and placed into the instrument's sample cuvette (10 × 10 × 45 mm), and the data were analyzed. Additionally, 3 mL of the prepared sample was filtered using a 0.22 µm filter [11].

2.4. Characterization by SEM

Information on morphology and particle size was obtained using a TESCAN VEGA3 scanning electron microscope (SEM, 15 kV, Brno, South Moravia, Czech Republic). Before SEM analysis, all samples were coated by sputtering with gold (99.999%) at 16 mA for 4 min using an SPI-MODULE sputtering coater (West Chester, PA, USA) [28].

2.5. Characterization by AFM

Particle size and morphology were determined using an atomic force microscope (AFM, model TT-AFM-WORKSHOP, Hilton Head Island, CA, USA). For that, 1 mg of C-Ag Ps was dissolved in a 100 mL volumetric flask containing an aqueous acetic acid solution (1% v/v). A drop was placed on a plastic tape substrate; after the solvent evaporated, the sample was analyzed using an AFM [11]. The AFM 15 µm software version 2012 (Hilton Head Island, CA, USA) was started; the camera was focused, and a small tip (radius < 15 nm, material: single crystal silicon, cantilever length: 215–235 µm) was brought close to the sample to carry out the analysis. Particle size was measured using 2D and 3D images in Gwyddion software (version 2013; Brno, Southern Moravia, Czech Republic).

2.6. Characterization of C-Ag Ps by FTIR

To identify the functional groups of the C-Ag Ps, potassium bromide (KBr) was dried in a Yamato drying oven (model DX402C, Chongqing, Beibei District, China) for 24 h at 100 °C [20].

0.5 mg of C-Ag Ps and 1 g of KBr were weighed on an Explorer OHAJJS digital analytical balance (model E12140, Parsippany, NJ, USA); the two substances were mixed and ground using a porcelain mortar. Once the two substances were homogenized, this sample was placed in a compression die to form a pellet, which was then placed in the iD1 accessory of the Thermo Scientific Nicolet iS5 Fourier-transform infrared (FTIR) spectrometer, with a standard resolution of 0.8 cm^{-1}, using OMNIC software version 2012 (Madison, WI, USA). The range was from 4000 to 400 cm^{-1} to identify chemical interactions between the biopolymer and the metal [22].

2.7. X-Ray Diffraction (XRD)

A Bruker D8 diffractometer (Advance ECO model, Billerica, MA, USA) was used with CuK-α radiation ($\lambda = 1.54$ Å) over a 2θ range of 10° to 80° and a scan rate of 0.02%, equipped with a D-teX Ultra detector, operating at an intensity of 35 kV and a current of 25 mA. X-ray diffraction (XRD) was performed on the C-Ag Ps; this method reveals the material's internal structure and determines whether it is crystalline, amorphous, or a combination of both [17].

2.8. Thermogravimetric Analysis of C-Ag Ps

The C-Ag Ps were also analyzed using thermogravimetric analysis (TGA), a thermal analysis method that measures a sample's mass over time as temperature changes or at

a constant temperature. The equipment used for this analysis was a thermogravimetric analyzer (TGA) manufactured by TA Instruments (model Q500, New Castle, PA, USA). The operating conditions were a heating rate of 10 °C min^{-1} in a nitrogen atmosphere with a gas flow rate of 50 mL min^{-1} over the temperature range from 25 to 600 °C; after 600 °C, an oxygen atmosphere was used to achieve complete combustion of the organic material [27].

2.9. Testing of C-Ag Ps Against the Bacterium Bacillus halotolerans MCC1

Agar dissolved in seawater was sterilized in an autoclave (model CV-250, Tecamac de Felipe Villanueva, Estado de Mexico, Mexico) at 121 °C and 1.05 bar for 15 min. In each Petri dish, a 1.2 cm diameter Whatman paper disc was used as the control and contained 1% *v*/*v* aqueous acetic acid solution. The C-Ag Ps were dissolved in 1% aqueous acetic acid and made up to 100 mL. Three different solution concentrations were prepared: 0.05, 0.10, and 0.15 mg mL^{-1}. The discs were immersed in the C-Ag Ps solutions. We prepared three Petri dishes; in each dish, we placed four discs: the first served as a blank, the second was for 0.05 mg mL^{-1}, the third for 0.10 mg mL^{-1}, and the fourth for 0.15 mg mL^{-1}. To measure the inhibition halos, Microsoft PowerPoint software, version 16.014334.20918 from Microsoft 365 (2024), was used with the ruler feature. The bacterium *Bacillus halotolerans* MCC1 is endemic to the Sea of Cortes off the coast of Sonora, Mexico, and is responsible for biofouling reverse osmosis membrane modules. It is capable of sporulation. It was removed and extracted using a physical treatment system with microfiltration and ultrafiltration membranes. The concentration of the bacterium *Bacillus halotolerans* MCC1 was 5.76×10^9 $CFUmL^{-1}$, measured using a Marienfeld Neubauer chamber, model Bright-Line Hemocytometer (Lauda, Baden-Württemberg, Germany), and a Zeigen photonic microscope, model VIRTUE-INF-PL-3 (Cuauhtémoc, Mexico City, Mexico). The extracted bacterium, *Bacillus halotolerans* MCC1, was inoculated onto Petri dishes using a sterilized loop in a laminar flow hood sterilized with UV light and alcohol. The dishes were incubated at 30 °C and monitored at 24 h [27].

3. Results and Discussion

3.1. Dynamic Light Scattering

Figure 2 shows the DLS results. Figure 2a represents a filtered aqueous particle dispersion, while Figure 2b shows an unfiltered aqueous particle dispersion. In Figure 2a, we used a filter with an average pore diameter of 220 nm; DLS yielded an average particle diameter of 168.8 nm, with a particle size range of 17–550 nm and a peak distribution of 5.2% (PDI = 0.27). In Figure 2b, the average particle diameter was 400 nm, but the solution was not filtered; therefore, the measured particle diameter was larger. However, the size range varied from 260 to 600 nm, with a 16% distribution (PDI = 0.034). Results similar to those of Villegas-Peralta et al. (2019) [11] were obtained, with DLS values of 315.5 nm and 437.4 nm for particles from pure chitosan. In another study by Armendariz-Ontiveros et al. (2022) [17], the researchers synthesized C-Ag NPs using the ionic gelation method and obtained particle diameters by DLS ranging from 80 to 200 nm by varying the molecular weight of the chitosan.

The particle diameter in the unfiltered sample (Figure 2b) suggests that, during ionic gelation synthesis, some particles may have aggregated due to electrostatic interactions between the chitosan chains and the silver ions [6], a common phenomenon in colloidal systems where pH or ionic strength is not strictly controlled [29]. In this regard, agglomeration can be explained by electrostatic attraction between particles with opposite surface charges or by reduced repulsion as medium conditions (ionic strength, concentration, or viscosity) change. According to Cavallaro et al. (2021) [30,31], chitosan's tendency to form three-dimensional networks via hydrogen bonding and Van der Waals forces may

promote the aggregation of metal nanoparticles, generating aggregates that increase the hydrodynamic size as measured by DLS.

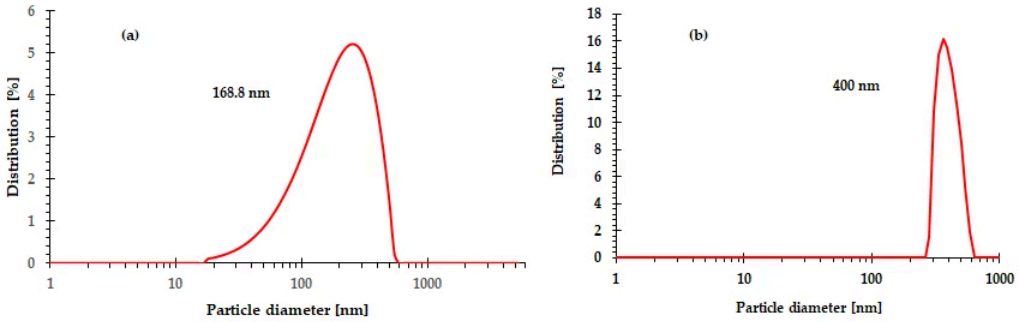


Figure 2. DLS analysis of C-Ag Ps: (**a**) filtered sample and (**b**) unfiltered sample.

3.2. Scanning Electron Microscopy

Figure 3 shows an SEM micrograph of the C-Ag Ps; the average particle size was 116.92 nm ± 39.78, measured on a 2 µm scale. SEM provided morphological information, revealing regular, semi-spherical particles, as observed in other studies [6–8,11,17]. SEM analysis revealed that the silver particles within the chitosan matrix tend to agglomerate; nevertheless, they are uniformly distributed throughout the synthesized material. Rizwan et al. (2023) [32] noted that, in nanoparticle synthesis, agglomeration and the distribution of NPs are attributed to the matrix—in this study, according to the amount of biopolymer used and the applied methodology—which results in reduced coverage and stabilization of the particles, because a weight ratio of 0.73 (*w*/*w*, $AgNO_3$/chitosan) was used in the preparation of the C-Ag Ps. Similarly, Álvarez-Sánchez et al. (2024) [28] analyzed ZnO NPs distributed and anchored in a polymer membrane via interfacial polymerization. The minimum size of the ZnO NPs was 100 nm, but when the membranes were doped with the NPs, they formed agglomerates measuring 350–500 nm, as detected by SEM. This suggests that interactions between the membrane and the particles play a key role in agglomeration. Similarly, Torres-Valenzuela et al. (2022) [25] used interfacial polymerization to dope polymeric membranes with silver nanoparticles with particle diameters of less than 100 nm. SEM characterization of the Ag NP-doped membrane surface revealed agglomerates.

3.3. Atomic Force Microscopy

Figure 4 shows micrographs obtained using 2D and 3D atomic force microscopy. Figure 4a reveals particles of various sizes; however, the particle size range is from 280 nm to 680 nm, with an average particle size of 495.7 nm ± 164. The particle size is similar to the results obtained by DLS. The particle morphology is hemispherical or elliptical, which is consistent with the SEM findings. The 2D and 3D results indicate that the particles were well distributed because they are sufficiently separated from one another, with an average distance of 4.4 µm ± 2.6. Zienkiewicz-Strzałka et al. (2020) [33] successfully visualized Ag nanoparticles using 3D AFM imaging; the Ag NPs measured between 20 and 50 nm, had a spherical morphology, and showed no agglomeration in chitosan/silica nanofibers. Wood et al. (2024) [34] analyzed Au NPs using AFM. The micrographs show individual nanoparticles and agglomerates of Au nanoparticles. A 5 µm scanner was used. The micrographs visualized agglomerates ranging from 300 to 500 nm and nanoparticles ranging from 50 to 100 nm.

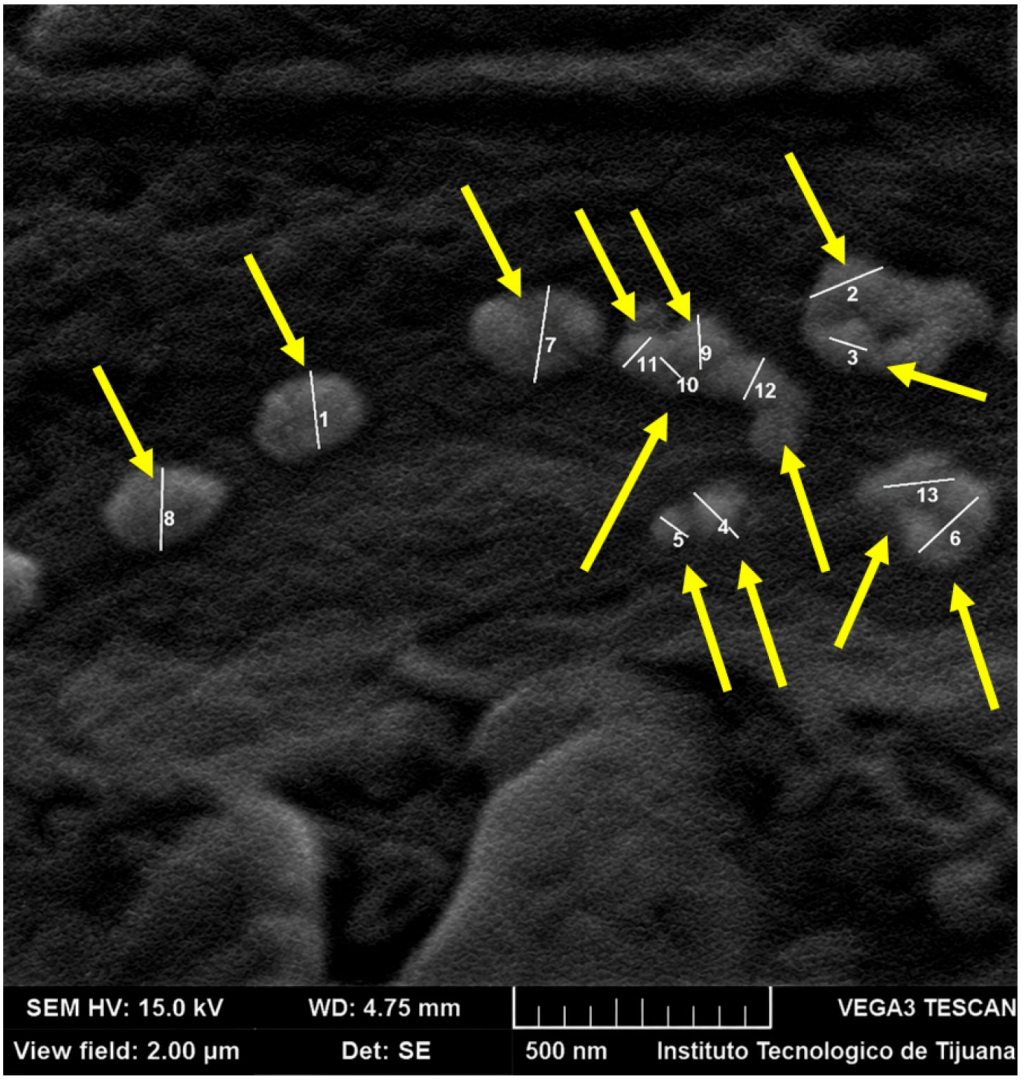


Figure 3. SEM analysis of the C-Ag Ps. The yellow arrows indicate the particle locations.

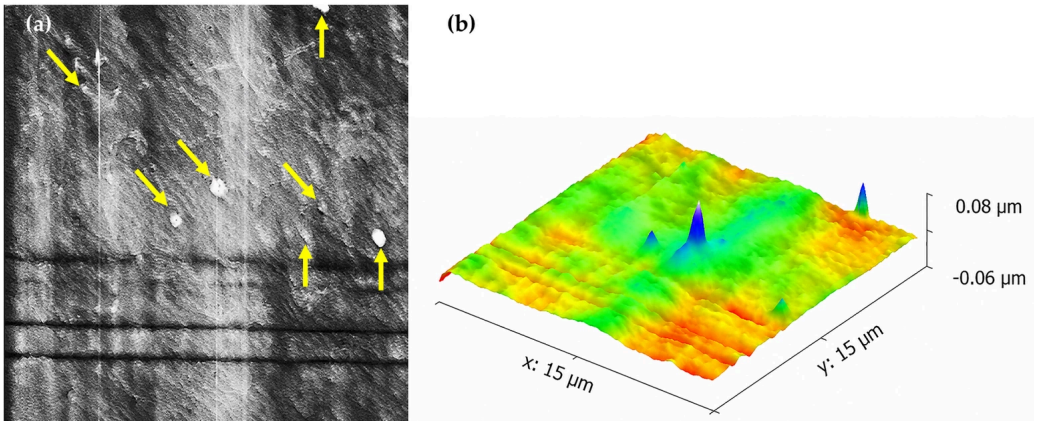


Figure 4. 15 µm scanning AFM analysis of C-Ag Ps: (**a**) 2D and (**b**) 3D. The yellow arrows indicate the particle locations.

Farkas et al. (2019) [35] used gold nanoparticles coated with PEG-PEI (polyethylene glycol-polyethyleneimine) and DNA-PEI nanoparticles coated with PEG, both with a core–shell architecture; AFM detected nanoparticle agglomerates ranging from 400 to 500 nm

and exhibiting a semispherical morphology, similar to the results in this study. Based on the background discussed and the results of this study, AFM allows visualization of particle size at the nanoscale.

3.4. Fourier-Transform Infrared Spectroscopy (FTIR)

This is observed in the FTIR spectra of chitosan (Figure 5a) and C-Ag Ps (Figure 5b). Chitosan exhibited a band at 3414.41 cm^{-1} due to the stretching of the hydroxyl (-OH) and amino (-NH_2) groups. In this same functional group region, the nanoparticles showed a greater wavenumber shift, with a band at 3420.57 cm^{-1}, slightly higher than that of chitosan, due to the presence of Ag [36]. In addition, the nanoparticles showed pronounced peaks at 1399.32 cm^{-1} and 1647.03 cm^{-1}, whereas chitosan showed peaks at 1400.69 cm^{-1} and 1657.65 cm^{-1}, suggesting narrower peaks for the -$CONH_2$ functional groups in the particles. According to Ogungbesan et al. (2024) [37], the incorporation of Ag NPs into a chitosan matrix changed the -OH/-NH_2 bands, resulting in a shift due to hydrogen bonding, as well as the C–O–C band was also shifted, as in the present study. Furthermore, differences were observed in the shape and intensity of the C–Ag Ps bands appearing at 1235, 1166, and 896 cm^{-1}, compared to chitosan alone. According to the literature, these signals can be attributed to the presence of phosphate groups from TPP present in the particles [38].

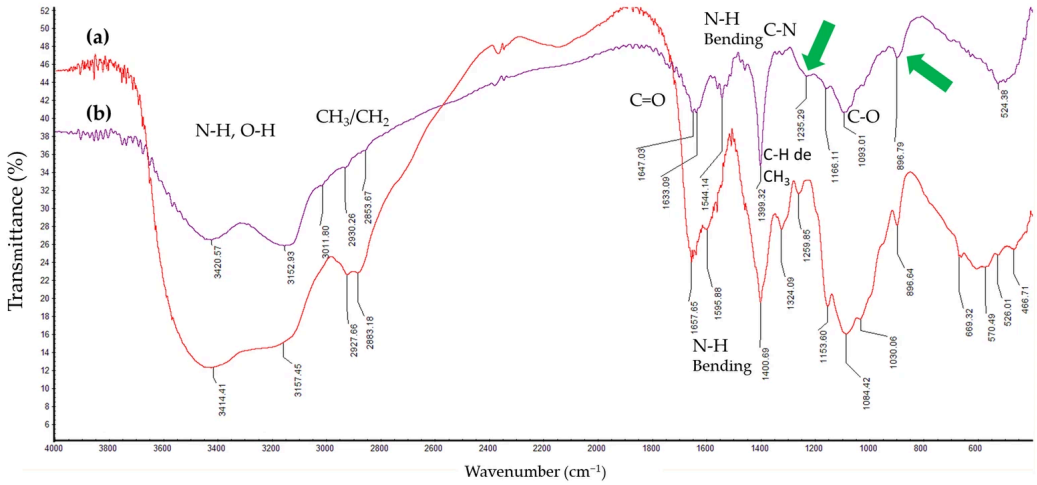


Figure 5. Comparative FTIR spectra of: (**a**) chitosan and (**b**) C-Ag Ps.

The 610 cm^{-1} signal of chitosan shifted to 524.38 cm^{-1} in the C-Ag Ps due to the interaction between Ag and chitosan (Figure 5). The peak intensities between 1000 cm^{-1} and 1350 cm^{-1}, due to C–N stretching and bending, are greatly reduced in silver-loaded chitosan particles because of the complex formed between chitosan and silver [25]. A similar phenomenon occurred for the amino and hydroxyl groups due to complexation with Ag metal [37].

3.5. Characterization by X-Ray Diffraction

The XRD pattern of the C-Ag Ps (Figure 6) showed a broad band around 20°, attributed to the semicrystalline nature of chitosan [39]. This peak is reduced because chitosan forms part of an amorphous matrix that decreases its crystallinity when incorporated into the nanoparticle within a cross-linked matrix. The signal at 11.16° shows a higher-intensity peak than the other signals, suggesting higher crystallinity [40]. Chitosan has the JCPDS PDF entry 39-1894, and AgCl has the JCPDS PDF entry 31-1238. The peaks at 27.94°, 32.25°, 46.37°, 55°, 57°, and 67° indicate that the Q-Ag particles contain AgCl. The Q-Ag particles consist of a chitosan matrix and AgCl.

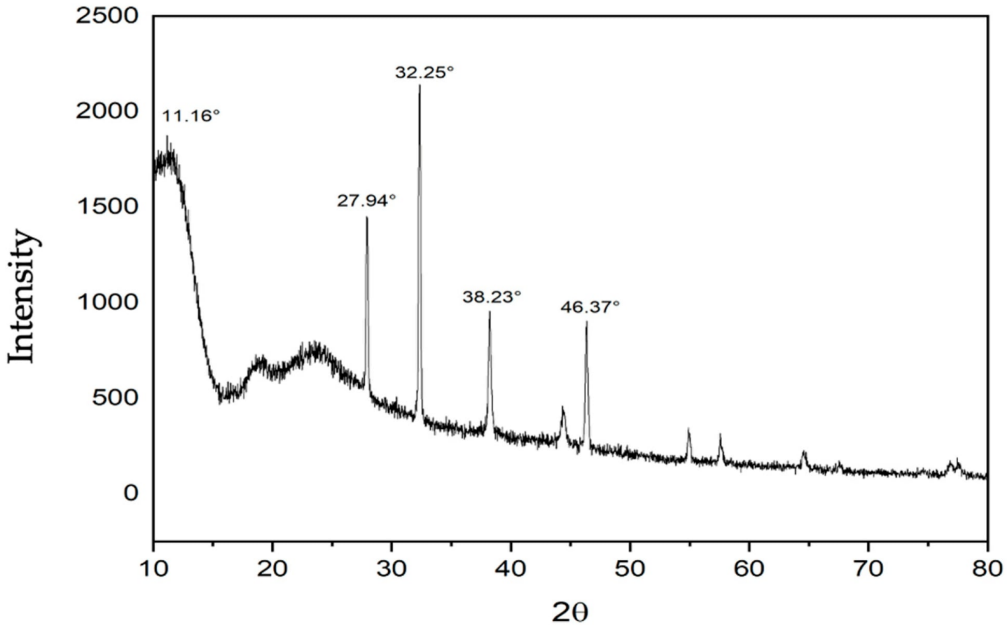


Figure 6. X-ray diffraction (XRD) patterns of C-Ag Ps.

3.6. Thermogravimetric Analysis of C-Ag Ps

Figure 7 shows the thermogravimetric analysis, which revealed two main stages of mass loss for the C-Ag Ps. The first stage occurred from 25 to 175 °C, with an inflection point at 111.1 °C, representing a 11.52% loss attributed to the removal of adsorbed water and water bound via hydrogen bonds to the amino and hydroxyl groups of chitosan. Ogungbesan et al. (2024) [37] reported an 11% mass loss in chitosan films over 30 to 160 °C. The second stage, with a maximum degradation temperature of 216.9 °C, involved a mass loss of 35.79%, corresponding to the depolymerization of chitosan, the breaking of glycosidic bonds, and the degradation of the polymer's functional groups; this is consistent with Türk et al. (2024) [41], who attribute the weight loss to the loss of water, amine, and CH_2OH molecules. Finally, the material exhibited a residue of 52.66% at 600 °C, considerably higher than that reported for pure chitosan by Türk et al. (2024) and Chelminiak-Dudkiewicz et al. (2022), indicating a thermally stable inorganic fraction attributable to residual mass generated during pyrolysis [37,41,42]. According to the literature on chitosan nanoparticles cross-linked with TPP via ionic gelation, the range of carbon and other residues is 30 to 48 percent. The article by Metway et al. (2023) indicates that CS/TPP NPs exhibit approximately 70% mass loss, which implies approximately 30% residual mass [43–45].

3.7. Tests Exploratory Against Bacillus halotolerans MCC1

The antibacterial activity of C-Ag Ps is shown in Figure 8, with evaluations at 0 and 24 h at concentrations of 0.05, 0.1, and 0.15 mg mL^{-1}. Table 1 shows inhibition zone diameters at 24 h. The disk diameter was 1.2 cm, and the resulting inhibition zones measured 1.425, 1.858, and 2.084 cm at 0.05, 0.1, and 0.15 mg mL^{-1}, respectively. Considering only the inhibition zone (zone minus disk diameter), the distance between the disc containing C-Ag Ps and bacterial colonies (DBC) was approximately 0.411, 0.658, and 0.884 cm at 0.05, 0.1, and 0.15 mg mL^{-1}, respectively. Since the highest concentration reflects the greatest antibacterial activity, these results indicate that the inhibitory effect increases; similarly, Tharani et al. (2020) [46] demonstrated that the Q-Ag NPs they synthesized exhibited antimicrobial activity against the Gram-positive bacterium *Bacillus subtilis*. They used a 10 µL volume, achieving a 6 mm zone of inhibition, and a 20 µL volume (1 mg mL^{-1}), achieving an 8 mm

zone of inhibition, indicating that higher concentrations of Q-Ag NPs resulted in greater antimicrobial activity [46].

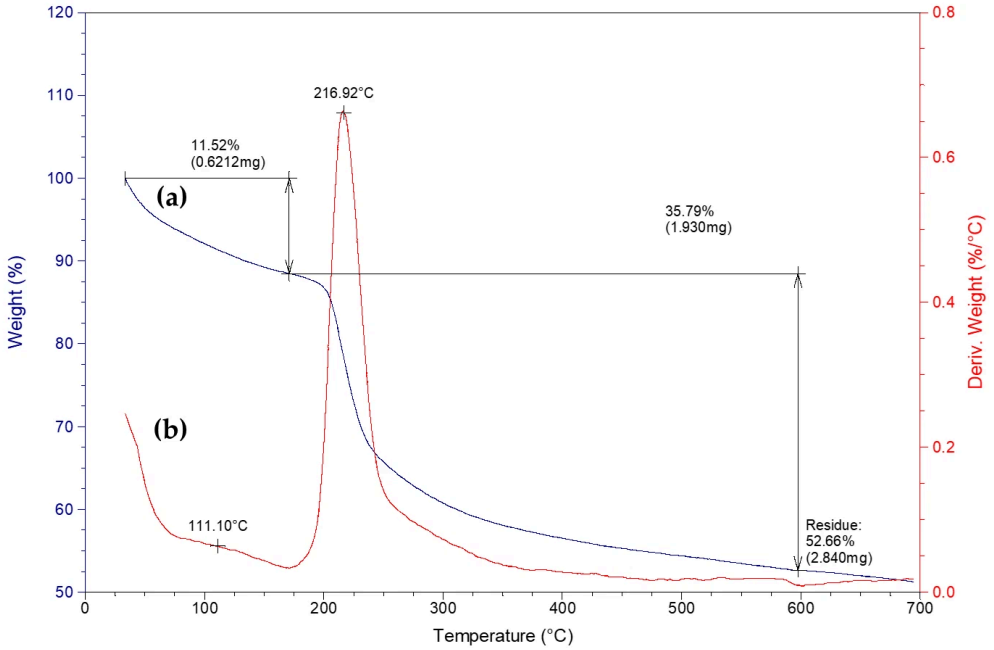


Figure 7. (**a**) Thermogravimetric analysis of C-Ag Ps (TGA, blue line) and (**b**) thermogravimetric derivation (DTG, red line).

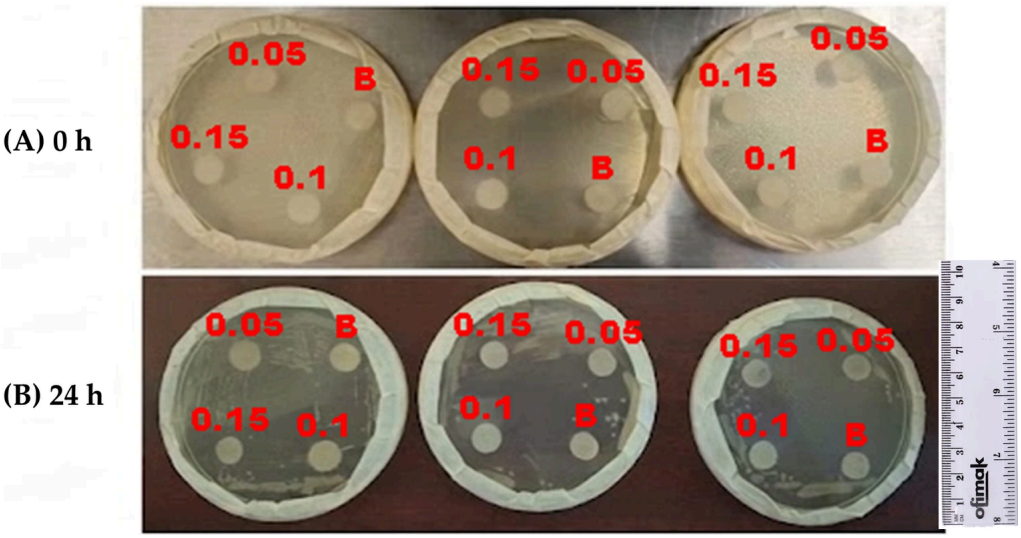


Figure 8. (**A**) Time 0 h and (**B**) time 24 h of antibacterial assays (*Bacillus halotolerans* MCC1) of C-Ag Ps at concentrations of 0.05, 0.10, and 0.15 mg mL^{-1} (B is the control).

Table 1. Inhibition zones of C-Ag Ps against *Bacillus halotolerans* MCC1 at 24 h.

C-Ag Ps Concentration (mg mL^{-1})	DBC * (cm)	SD ** (cm)
0.05	0.411	± 0.10
0.10	0.658	± 0.23
0.15	0.884	± 0.19

* DBC: distance between the disc containing C-Ag Ps and bacterial colonies. ** DS: Standard Deviation.

The approximately 2.15-fold increase between 0.05 and 0.15 mg mL^{-1} confirms a dose-dependent response, which is characteristic of antimicrobial materials. During the first 24 h, inhibition zones around the particle-containing discs are clearly observed, whereas the control (1% aqueous acetic acid) shows no comparable inhibition, indicating that the antibacterial effect stems primarily from the particles.

The DBC increase in size with increasing concentration can be explained by several synergistic mechanisms between chitosan and silver. Chitosan has protonated amino groups that interact electrostatically with anionic components of the bacterial cell wall [16,26], promoting particle adsorption onto the bacterial surface. This interaction increases cell membrane permeability and facilitates the penetration of silver ions and particles into the cell interior. Wang et al. (2017) [47] reported in their review that metal nanoparticles can penetrate biofilms and exert antibacterial activity through various mechanisms. They interact with bacteria through electrostatic, Van der Waals, hydrophobic, and receptor–ligand forces. Subsequently, they affect the membrane and cellular components, causing oxidative stress, enzymatic alterations, and genetic changes [47].

Overall, the results show that C-Ag Ps exhibit high antibacterial efficacy against *Bacillus halotolerans* MCC1 and that this activity depends on concentration. The 0.15 mg mL^{-1} concentration produced inhibition, followed by 0.10 mg mL^{-1} and 0.05 mg mL^{-1}, confirming that increasing the dose increases the availability of bioactive silver. This trend toward higher C-Ag Ps concentrations suggests that modifying the surface of reverse osmosis membranes could impart antibiofouling properties.

4. Conclusions

C-Ag Ps were successfully synthesized using the ionic gelation technique; DLS and SEM showed an average diameter C-Ag Ps filtered of 168.8 nm and 116.92 nm meanwhile AFM and DLS showed an average without filtration of 400 and 495.7 nm, respectively. In addition, SEM provided morphological information on the NPs, revealing semispherical, uniform particles. FTIR provided evidence of changes in the chemical environment of chitosan functional groups because the signals were influenced by clustering of chitosan polymer chains and interactions between silver and chitosan functional groups (-NH_2 and -OH). XRD results suggest the formation of a chitosan/Ag composite with crystalline phases dispersed in a polymer matrix. TGA analysis showed that the C-Ag Ps left an inorganic residue of 52.66% at 600 °C, attributable to silver, residual carbon and ashes. Performance testing of the C-Ag Ps against the bacterium *Bacillus halotolerans* MCC1 showed that the particles had antibacterial properties and inhibited the bacterium's growth. Hence, the synthesized particles could have potential for future evaluation as an antimicrobial additive.

Author Contributions: V.A.A.-M. experimental work related to the synthesis and characterization of nanoparticles; J.Á.-S., conceptualization, experimental methodology, experimental work related to the synthesis and characterization of nanoparticles, writing—original draft preparation, validation, and funding acquisition; G.E.D.-I., conceptualization, experimental work related to synthesis of nanoparticles, writing of the manuscript, and funding acquisition; Y.V.-P., supervision and funding acquisition; R.G.S.-D., supervision, editing and preparation of the manuscript, funding acquisition; B.G.G.-G., supervision and funding acquisition; S.P.-S., characterization nanoparticles, supervision, revision, and editing. All authors have read and agreed to the published version of the manuscript; L.A.P.-C., supervision, editing, and manuscript preparation, funding acquisition.

Funding: This research was funded by the Instituto Tecnologico de Sonora through PROFAPI funded projects: 2026-046 and CA-2026-002; and further, through the CONAHCYT Frontier Science project CBF-G-2025-1036. We also thank the Academic Capacity and Competitiveness Program of the Natural Resources Department.

Data Availability Statement: The original contributions presented in the study are included in the article, further inquiries can be directed to the corresponding author.

Acknowledgments: The authors acknowledge SECIHTI for the scholarship awarded to the graduate student V.A.A.-M.

Conflicts of Interest: The authors declare no conflicts of interest.

References

1. Alarcón, H.; Tolmos, M.; Villacrés, N.; Huarote, E. Química verde—Una alternativa eco-amigable en la obtención de nanopartículas de Ag0. *Rev. Soc. Quím. Peru* **2021**, *87*, 298–306. [CrossRef]
2. Alcázar-Medina, F.A.; Valle-Cervantes, S.; Alcazar-Medina, T.; Rodríguez-Rosales, M.D.J. Optimization of copper removal through spherical agglomeration: Effect of pH precipitation and the use of Agavespp. leaf extracts as biosurfactants. *Rev. Mex. Ing. Quim.* **2024**, *23*, 71–84. [CrossRef]
3. Senthilkumar, P.; Yaswant, G.; Kavitha, S.; Chandramohan, E.; Kowsalya, G.; Vijay, R.; Sudhagar, B.; Kumar, D.R.S. Preparation and characterization of hybrid chitosan-silver nanoparticles (Chi-Ag NPs); A potential antibacterial agent. *Int. J. Biol. Macromol.* **2019**, *141*, 290–298. [CrossRef] [PubMed]
4. Álvarez-Chimal, R.; Arenas-Alatorre, J.Á.; Marichi-Rodríguez, F.; Correa-Prado, R.; Álvarez-Pérez, M.A. La química verde en la síntesis de nanopartículas y sus propiedades antibacterianas. *Mundo Nano. Rev. Interdiscip. Nanociencias Nanotecnología* **2025**, *18*, e69826. [CrossRef]
5. Bayda, S.; Adeel, M.; Tuccinardi, T.; Cordani, M.; Rizzolio, F. The history of nanoscience and nanotechnology: From chemical-physical applications to nanomedicine. *Molecules* **2019**, *25*, 112. [CrossRef] [PubMed]
6. Nie, J.; Wang, Z.; Hu, Q. Chitosan Hydrogel Structure Modulated by Metal Ions. *Sci. Rep.* **2016**, *6*, 36005. [CrossRef] [PubMed]
7. Ijaz, I.; Gilani, E.; Nazir Y, A.; Bukhari, A. Detail review on chemical, physical and green synthesis, classification, characterizations and applications of nanoparticles. *Green Chem. Lett. Rev.* **2020**, *13*, 223–245. [CrossRef]
8. Kučuk, N.; Primožič, M.; Knez, Ž.; Leitgeb, M. Sustainable biodegradable biopolymer-based nanoparticles for healthcare applications. *Int. J. Mol. Sci.* **2023**, *24*, 3188. [CrossRef] [PubMed]
9. Azeez, S.; Sabapathy, P.C.; Nagarajan, S.; Ramalingam, S.; Anusha, N.; Sathiyaseelan, A. Sustainable industrial applications of chitosan and chitosan-based nanomaterials: Advances, challenges, and future perspectives. *Resour. Chem. Mater.* **2026**, *5*, 100214. [CrossRef]
10. Tellez-Barrios, G.; Cadenas-Pliego, G.; Toledo-Manuel, I.; Pérez-Alvarez, M.; Alvarado-Canche, C.N.; Mancillas-Salas, S.; Andrade-Guel, M.; Mata-Padilla, J.M.; Cabello-Alvarado, C.J. Surface Modification of TiO_2 and ZrO_2 Nanoparticles with Organic Acids and Ultrasound to Enhance Antibacterial Activity. *Materials* **2025**, *18*, 2786. [CrossRef] [PubMed]
11. Villegas-Peralta, Y.; Correa-Murrieta, M.A.; Meza-Escalante, E.R.; Flores-Aquino, E.; Ál-varez-Sánchez, J.; Sánchez-Duarte, R.G. Effect of the preparation method in the size of chitosan nanoparticles for the removal of allura red dye. *Polym. Bull.* **2019**, *76*, 4415–4430. [CrossRef]
12. Silva, N.C.; Chevigny, C.; Domenek, S.; Almeida, G.; Assis, O.B.G.; Martelli-Tosi, M. Nanoencapsulation of active compounds in chitosan by ionic gelation: Physicochemical, active properties and application in packaging. *Food Chem.* **2025**, *463*, 141129. [CrossRef] [PubMed]
13. Pereira Parchen, G.; Quaillet, M.; Alves de Freitas, R.; Hillaireau, H. Chitosan-based nano-objects for drug delivery: A review of their chemical modifications, supramolecular organization and biological fate. *RSC Pharm.* **2025**, *2*, 1292–1322. [CrossRef]
14. Shahalaei, M.; Azad, A.K.; Sulaiman, W.M.A.W.; Derakhshani, A.; Mofakham, E.B.; Mallandrich, M.; Kumarasamy, V.; Subramaniyan, V. A review of metallic nanoparticles: Present issues and prospects focused on the preparation methods, characterization techniques, and their theranostic applications. *Front. Chem.* **2024**, *12*, 1398979. [CrossRef] [PubMed]
15. Hajra, K.; Maity, D.; Saha, S. Recent advancements of metal oxide nanoparticles and their potential applications: A review. *Adv. Mater. Lett.* **2024**, *15*, 2401-1740. [CrossRef]
16. Villegas-Peralta, Y.; Gonzalez Tineo, P.A.; Sánchez-Duarte, R.G.; Aguilar-Ruiz, A.A. Obtención de papel de quitosano a partir de cáscara de camarón. *Rev. Ing.-Nova* **2024**, *3*, 34–47. [CrossRef]
17. Armendáriz-Ontiveros, M.M.; Villegas-Peralta, Y.; Madueño-Moreno, J.E.; Álvarez-Sánchez, J.; Dévora-Isiordia, G.E.; Sánchez-Duarte, R.G.; Madera-Santana, T.J. Modification of Thin Film Composite Membrane by Chitosan–Silver Particles to Improve Desalination and Anti-Biofouling Performance. *Membranes* **2022**, *12*, 851. [CrossRef] [PubMed]
18. Anju, A.B.; Gopal, K.S.; Panchami, P.S.; Vijayaraghavan, R. A simple and user-friendly protocol for chitosan nanoparticle synthesis. *Discov. Nano* **2025**, *20*, 211, Corection in *Discov. Nano* **2025**, *20*, 222. [CrossRef] [PubMed]
19. Magdolenova, Z.; Collins, A.; Kumar, A.; Dhawan, A.; Stone, V.; Dusinska, M. Mechanisms of genotoxicity. A review of in vitro and in vivo studies with engineered nanoparticles. *Nanotoxicology* **2014**, *8*, 233–278. [CrossRef] [PubMed]

20. Shaban, N.Z.; Aboelsaad, A.M.; Shoueir, K.R.; Abdulmalek, S.A.; Awad, D.; Shaban, S.Y.; Mansour, H. Chitosan-based dithiophenolato nanoparticles: Preparation, mechanistic information of DNA binding, antibacterial and cytotoxic activities. *J. Mol. Liq.* **2020**, *318*, 114252. [CrossRef]
21. Laanoja, J.; Sihtmae, M.; Vija, H.; Kurvet, I.; Otsus, M.; Smits, K.; Kahru, A.; Kasemets, K. Particle-driven synergistic antibacterial effect of silver–chitosan nanocomposites against Escherichia coli, Pseudomonas aeruginosa, and Staphylococcus aureus. *ACS Omega* **2025**, *10*, 27904–27919. [CrossRef] [PubMed]
22. Yao, C.J.; Yang, S.J.; Shieh, M.J.; Young, T.H. Development of a chitosan-silver nanocomposite/β-1, 3-glucan/hyaluronic acid composite as an antimicrobial system for wound healing. *Polymers* **2025**, *17*, 350. [CrossRef] [PubMed]
23. El-Sheikh, M.A.; Abdeldayem, S.A. A novel photo-induced synthesis of carboxymethyl chitosan-silver nanocomposite: Preparation, characterization and antibacterial efficacy of cotton finished fabrics. *Sci. Rep.* **2026**, *16*, 5347. [CrossRef] [PubMed]
24. Suresh, D.; Goh, P.S.; Wong, T.W.; Zhang, L.; Ismail, A.F. In-situ complexation of silver nanoparticle on thin film composite reverse osmosis membrane for improving desalination and anti-biofouling performance. *Desalination* **2024**, *569*, 117040. [CrossRef]
25. Torres-Valenzuela, P.G.; Álvarez-Sánchez, J.; Dévora-Isiordia, G.E.; Armendáriz-Ontiveros, M.M.; del Rosario Martínez-Macias, M.; Pérez-Sicairos, S.; Fimbres Weihs, G.A. Modification and characterization of TFC membranes with Ag nanoparticles: Application in seawater desalination. *Polym. Bull.* **2023**, *80*, 6285–6306. [CrossRef]
26. Ali, S.W.; Rajendran, S.; Joshi, M. Synthesis and characterization of chitosan and silver loaded chitosan nanoparticles for bioactive polyester. *Carbohydr. Polym.* **2011**, *83*, 438–446. [CrossRef]
27. Villegas-Peralta, Y.; López-Cervantes, J.; Madera Santana, T.J.; Sánchez-Duarte, R.G.; Sánchez-Machado, D.I.; Martínez-Macías, M.d.R.; Correa-Murrieta, M.A. Impact of the molecular weight on the size of chitosan nanoparticles: Characterization and its solid-state application. *Polym. Bull.* **2021**, *78*, 813–832. [CrossRef]
28. Álvarez-Sánchez, J.; Dévora-Isiordia, G.E.; Muro, C.; Villegas-Peralta, Y.; Sánchez-Duarte, R.G.; Torres-Valenzuela, P.G.; Pérez-Sicairos, S. Improved Flux Performance in Brackish Water Reverse Osmosis Membranes by Modification with ZnO Nanoparticles and Interphase Polymerization. *Membranes* **2024**, *14*, 207. [CrossRef] [PubMed]
29. Nilsen-Nygaard, J.; Strand, S.P.; Vårum, K.M.; Draget, K.I.; Nordgård, C.T. Chitosan: Gels and Interfacial Properties. *Polymers* **2015**, *7*, 552–579. [CrossRef]
30. Cavallaro, G.; Micciulla, S.; Chiappisi, L.; Lazzara, G. Chitosan-based smart hybrid materials: A physico-chemical perspective. *J. Mater. Chem. B* **2021**, *9*, 594–611. [CrossRef] [PubMed]
31. Geetha, K.; Yekkala, M.; Kiran, R.S. A review of revolutionizing green synthesis of nanoparticles in pharmacy and healthcare. *J. Pharm. Res. Int.* **2024**, *36*, 25–40. [CrossRef]
32. Rizwan, M.; Iqbal, N.; Iqbal, M.H.; Ali, A.; Khan, A.U.; Zafar, S.; Rehman, S. Synthesis of chitosan–silver nanocomposite and its evaluation as an antibacterial coating for mobile phone glass protectors. *ACS Omega* **2023**, *8*, 17699–17711. [CrossRef] [PubMed]
33. Zienkiewicz-Strzałka, M.; Deryło-Marczewska, A.; Skorik, Y.A.; Petrova, V.A.; Choma, A.; Komaniecka, I. Silver nanoparticles on chitosan/silica nanofibers: Characteriza-tion and antibacterial activity. *Int. J. Mol. Sci.* **2019**, *21*, 166. [CrossRef] [PubMed]
34. Wood, J.; Palms, D.; Dabare, R.; Vasilev, K.; Bright, R. AFM for Nanomechanical Assessment of Polymer Overcoatings on Nanoparticle-Decorated Biomaterials. *Nanomaterials* **2024**, *14*, 1475. [CrossRef] [PubMed]
35. Farkas, N.; Scaria, P.V.; Woodle, M.C.; Dagata, J.A. Physical-chemical measurement method development for self-assembled, core-shell nanoparticles. *Sci. Rep.* **2019**, *9*, 1655. [CrossRef] [PubMed]
36. Vanti, G.; Poondla, N.; Manogaran, P.; Teradal, N.; S, V.; Kaulgud, R.; Kurjogi, M. Synthesis and Characterization of Multifunctional Chitosan–Silver Nanoparticles: An In-Vitro Ap-proach for Biomedical Applications. *Pharmaceuticals* **2024**, *17*, 1229. [CrossRef] [PubMed]
37. Ogungbesan, S.O.; Buxaderas, E.; Adedokun, R.A.; Moglie, Y.; Grijalvo, S.; García, M.T.; Bingbing, C.; Díaz, D.D.; Fu, G. Synthesis and characterization of chitosan–silver nanocomposite film: Antibacterial and cytotoxicity study. *ChemistrySelect* **2024**, *9*, e202404909. [CrossRef]
38. Martins, A.F.; de Oliveira, D.M.; Pereira, A.G.; Rubira, A.F.; Muniz, E.C. Chitosan/TPP microparticles obtained by microemulsion method applied in controlled release of heparin. *Int. J. Biol. Macromol.* **2012**, *51*, 1127–1133. [CrossRef] [PubMed]
39. Hashem, A.H.; Shehabeldine, A.M.; Ali, O.M.; Salem, S.S. Synthesis of chitosan-based gold nanoparticles: Antimicrobial and wound-healing activities. *Polymers* **2022**, *14*, 2293. [CrossRef] [PubMed]
40. Carapeto, A.P.; Ferraria, A.M.; do Rego, A.M.B. Unraveling the reaction mechanism of silver ions reduction by chitosan from so far neglected spectroscopic features. *Carbohydr. Polym.* **2017**, *174*, 601–609. [CrossRef] [PubMed]
41. Türk, S.; Yılmaz, E.; Semerci, A.B.; Kırkbınar, M.; İbrahimoğlu, E.; Çalışkan, F. Development of dual-effect AW/Ag/CHI bioactive and antibacterial coating for orthopedic implant surfaces. *J. Therm. Anal. Calorim.* **2024**, *149*, 9119–9129. [CrossRef]
42. Chelminiak-Dudkiewicz, D.; Smolarkiewicz-Wyczachowski, A.; Mylkie, K.; Wujak, M.; Mlynarczyk, D.T.; Nowak, P.; Bocian, S.; Goslinski, T.; Ziegler-Borowska, M. Chitosan-based films with cannabis oil as a base material for wound dressing application. *Sci. Rep.* **2022**, *12*, 18658. [CrossRef] [PubMed]

43. Metwaly, A.M.; Abdel-Raoof, A.M.; Alattar, A.M.; El-Zomrawy, A.A.; Ashmawy, A.M.; Metwally, M.G.; Abu-Saied, M.A.; Lotfy, A.M.; Alsfouk, B.A.; Elkaeed, E.B.; et al. Preparation and characterization of patuletin-loaded chitosan nanoparticles with improved selectivity and safety profiles for anticancer applications. *J. Chem.* **2023**, *2023*, 6684015. [CrossRef]
44. Alehosseini, E.; Shahiri Tabarestani, H.; Kharazmi, M.S.; Jafari, S.M. Physicochemical, thermal, and morphological properties of chitosan nanoparticles produced by ionic gelation. *Foods* **2022**, *11*, 3841. [CrossRef] [PubMed]
45. Lazaridou, G.; Nenadis, N. Chitosan Nanoparticles Loaded with Alkaline-Released Rice Bran Hydroxycinnamic Acids: Physicochemical Characterisation, Antioxidant Activity and In Vitro Bioaccessibility. *Foods* **2026**, *15*, 3745. [CrossRef] [PubMed]
46. Tharani, S.; Bharathi, D.; Ranjithkumar, R. Extracellular green synthesis of chitosan-silver nanoparticles using Lactobacillus reuteri for antibacterial applications. *Biocatal. Agric. Biotechnol.* **2020**, *30*, 101838. [CrossRef]
47. Wang, L.; Hu, C.; Shao, L. The antimicrobial activity of nanoparticles: Present situation and prospects for the future. *Int. J. Nanomed.* **2017**, *12*, 1227–1249. [CrossRef] [PubMed]

Disclaimer/Publisher's Note: The statements, opinions and data contained in all publications are solely those of the individual author(s) and contributor(s) and not of MDPI and/or the editor(s). MDPI and/or the editor(s) disclaim responsibility for any injury to people or property resulting from any ideas, methods, instructions or products referred to in the content.